J Mol Model (2013) 19:4239–4249
DOI 10.1007/s00894-013-1862-4

ORIGINAL PAPER

Optical chemosensors for Cu(II) ion based on BODIPY derivatives: an experimental and theoretical study

Tasawan Keawwangchai · Banchob Wanno · Nongnit Morakot · Somchai Keawwangchai

Received: 15 October 2012 / Accepted: 18 April 2013 / Published online: 9 June 2013

Abstract Two BODIPY derivatives for Cu^{2+} ion chemosensors containing 4-[2-(diethylamino)-2-oxoethoxy]phenyl (**BDP1**) and 3,4-bis[2-(diethylamino)-2-oxoethoxy]phenyl (**BDP2**) were synthesized by coupling appropriate *N*,*N*-diethyl-2-(4-formylphenoxy)acetamide and 2,4-dimethylpyrrole moieties in the presence of trifluoroacetic acid and anhydrous dichloromethane at room temperature. The binding abilities between these chemosensors and 50 equivalents of Na^{+}, K^{+}, Ag^{+}, Ca^{2+}, Fe^{2+}, Ni^{2+}, Cu^{2+}, Zn^{2+}, Cd^{2+}, Hg^{2+} and Pb^{2+} ions were studied using UV-vis and fluorescence spectrophotometry. The results show that, compared to other ions, both the UV-vis absorption and fluorescence emission intensity of **BDP2** decreased dramatically when Cu^{2+} ion was added. To explain this behavior, ab initio quantum chemical calculations were performed using correlated second-order Møller-Plesset perturbation theory (MP2/LanL2DZ). The calculated orbital energies indicated that the decrease in UV-vis absorption intensity and the quenching of fluorescene emission were due to the single-electron reduction of Cu^{2+} to Cu^{+} ion.

Keywords BODIPY · Fluorescence · Chemosensor · DFT · MP2 · LanL2DZ

Electronic supplementary material The online version of this article (doi:10.1007/s00894-013-1862-4) contains supplementary material, which is available to authorized users.

T. Keawwangchai (✉) · B. Wanno
The Center of Excellence for Innovation in Chemistry (PERCH-CIC) and Supramolecular Chemistry Research Unit, Department of Chemistry, Faculty of Science, Mahasarakham University, Maha Sarakham 44150, Thailand
e-mail: k.tasawan@gmail.com

N. Morakot · S. Keawwangchai (✉)
Supramolecular Chemistry Research Unit, Department of Chemistry, Faculty of Science, Mahasarakham University, Maha Sarakham 44150, Thailand
e-mail: somchai2k@gmail.com

Introduction

The design of chemosensors capable of selectively recognizing particular metal ions has attracted much interest in recent years [1–3]. Such chemosensors are generally organic molecules comprising functional groups capable of binding metal ions—a binding subunit—and capable of giving a signal when a binding event occurs—a signaling subunit. The signaling subunit can be chosen to suit the required application; signaling mechanisms used include electrochemical [4, 5] or optical [6, 7] methods, or surface-enhanced Raman scattering (SERS) [8–11]. Of these, optical changes are attractive due to the simplicity of detection, which can be done with the naked eye or using rugged and cheap spectroscopic instrumentation [12–15].

One metal that has attracted particular interest in the field of chemosensor design is the copper ion [16–18]. Copper is an essential trace mineral of importance for both physical and mental health, and a cofactor that takes an active part in the activity of a large variety of enzymes [19–21]. As a consequence, Cu^{2+} plays an important role in fundamental physiological processes in all organisms. If levels of Cu^{2+} exceed cellular requirements, toxicity to biological systems can occur [22–24]. Thus, the development of new, selective, sensitive detection and optical chemosensors for Cu^{2+} in chemical and biological systems is actively investigated [25, 26].

In optical chemosensors, the signaling subunit can be either a chromophore or a fluorophore. Among these, 4,4-difluoro-4-bora-3a,4a-diaza-s-indacene (BODIPY) is very attractive due to its high molar absorptivity, high fluorescence quantum yields, and stability against light- and chemical-reactions. Moreover, its spectroscopic and photophysical properties can be fine-tuned by attachment of ancillary residues at the appropriate positions of the difluoroboron dipyrromethene core [27–30]. A mechanism often used to control the signaling of BODIPY-based chemosensors is the process of photoinduced electron

transfer (PET) [31–34]. In principle, PET can take place in two directions: from a donor to the excited-state fluorophore (reductive PET), or from an excited-state fluorophore to a binding subunit (oxidative PET). Both events are accompanied by quenching of the fluorophore emission.

This work attempted to design and synthesize an optical chemosensor for copper(II) ion. BODIPY was chosen as the signaling subunit, and 4-[2-(diethylamino)-2-oxoethoxy]phenyl or 3,4-bis[2-(diethylamino)-2-oxoethoxy]phenyl groups were chosen as the binding subunit. The optical changes upon binding with metal ions (Na^+, K^+, Ag^+, Ca^{2+}, Fe^{2+}, Ni^{2+}, Cu^{2+}, Zn^{2+}, Cd^{2+}, Hg^{2+} and Pb^{2+}) were observed using UV-vis and fluorescence spectrophotometries. Computational calculations were used to investigate the geometrical structures of these synthetic compounds and their complexes with metal ions. The binding energies and changes in the thermodynamic properties of complexation between chemosensors with Na^+, K^+, Ag^+, Ca^{2+}, Fe^{2+}, Ni^{2+}, Cu^{2+}, Zn^{2+}, Cd^{2+}, Hg^{2+} and Pb^{2+} ions were calculated using density functional theory (DFT).

Materials and methods

Reagents

Unless otherwise specified, all solvents and materials used were reagent grade and purchased from Fluka (Buchs, Switzerland), BHD (VWR, Radnor, PA), Aldrich (St. Louis, MO), Carlo Erba (Rodano, Italy), Merck (Darmstadt, Germany) or J.T. Baker (Phillipsburg, NJ) and were used without further purification. Commercial grade solvents such as acetone, dichloromethane, hexane, methanol and ethylacetate were purified by distillation before use. Acetonitrile and dichloromethane used for setting up the reaction were dried over calcium hydride and freshly distilled under nitrogen atmosphere prior to use. Column chromatography was carried out on silica gel (Kieselgel 60, 0.063–0.200 nm, Merck). Thin layer chromatography (TLC) was performed on silica gel plates (Kieselgel 60, F_{254}, 1 mm, Merck). Compounds on TLC plates were detected by UV-light. All manipulations were carried out under nitrogen atmosphere.

Synthesis

2-chloro-N,N-diethylacetamide, **3**

To a suspension of diethylamine (11.43 ml, 110 mmol), Na_2CO_3 (10.60 g) and ether (100 ml) at −10 °C was added chloroacetyl chloride (7.95 ml, 100 mmol). The reaction mixture was maintained below room temperature during the addition. The mixture was stirred for 45 min after the addition was complete. The solid was removed by filtration, and the filtrate was concentrated resulting in a residue. The residue was dissolved in CH_2Cl_2, extracted with 1 M HCl following by dilute Na_2CO_3 solution and dried over solid Na_2SO_4, which resulted in an organic layer. Concentration of the organic layer afforded a light yellow liquid. The residue was purified by distillation (60–70 °C, 2 mm Hg) to provide 8.18 g light yellow oil. The NMR spectrum of this light yellow liquid was consistent with the desired product and indicated that the compound was >95 % pure. ^{1}H-NMR spectrum (400 MHz, $CDCl_3$, ppm): δ 1.13–1.17 (t, 3H, CH_2CH_3, J=14 Hz), 1.23–1.27 (t, 3H, CH_2CH_3, J=14.4 Hz), 3.38–3.42 (q, 4H, NCH_2CH_3, J=14 Hz), 4.10 (s, 2H, $ClCH_2C$=O).

N,N-diethyl-2-(4-formylphenoxy)acetamide, **5a**

A suspension of 4-hydroxybenzaldehyde, **4a** (122 mg, 1 mmol), Na_2CO_3 (2.76 g) and 2-chloro-*N,N*-diethylacetamide, **3** (0.3 ml, 2 mmol) in CH_3CN 50 ml was refluxed overnight. The solid was removed by filtration. Subsequently, the filtrate was concentrated under reduced pressure resulting in a residue. The residue was dissolved in CH_2Cl_2 (100 ml), washed with 0.5 M HCl (100 ml), followed by water (200 ml). After drying with Na_2SO_4, the solvent was removed under reduced pressure. The crude product was purified by tritulation with MeOH to give compound **5a** in pale yellow oil. ^{1}H-NMR spectrum (400 MHz, $CDCl_3$, ppm): δ 1.13–1.16 (t, 3H, CH_2CH_3, J=14 Hz), 1.18–1.26 (t, 3H, CH_2CH_3, J=30.4 Hz), 3.38–3.42 (q, 4H, NCH_2CH_3, J=14.4 Hz), 4.80 (s, 2H, OCH_2C=O), 7.05–7.07 (d, 2H, Ar*H*, J=8.4 Hz), 7.83–7.85 (d, 2H, Ar*H*, J=9.2 Hz), 9.88 (s, 1H, ArC*H*O).

10-{4-[2-(diethylamino)-2-oxoethoxy]phenyl}-5,5-difluoro-1,3,7,9-tetramethyl-5H-dipyrrolo[1,2-c:2',1'-f][1–3]diazaborinin-4-ium-5-uide, **BDP1**

The *N,N*-diethyl-2-(4-formylphenoxy)acetamide, **5a** (504 mg, 2 mmol) and 2,4-dimethylpyrrole (0.42 ml, 4 mmol) were dissolved in anhydrous CH_2Cl_2 (160 ml) under N_2 atmosphere. Then, one drop of TFA was added to the solution, which was then stirred for 15 min at room temperature. A solution of 2,3-dichloro-5,6-dicyano-1,4-benzoquinone (DDQ, 454 mg, 2 mmol) in CH_2Cl_2 was added with a syringe, and the reaction was continued for another 2 h. Then Et_3N (2 ml) was added followed by BF_3OEt_2 (4 ml) during 30 min and stirred overnight. After concentrating under in vacuum, the residue was purified by column chromatography (silica, 5 % MeOH/CH_2C1_2) the desired product **BDP1** was obtained as a brown solid (314 mg, 33% yield). ^{1}H-NMR spectrum (400 MHz, $CDCl_3$, ppm): δ 1.12–1.16 (t, 3H, CH_2CH_3, J=14 Hz), 1.21–1.25 (t, 3H, CH_2CH_3, J=14 Hz), 1.41 (s, 6H, PyCH_3), 2.55 (s, 6H, PyCH_3), 3.42–3.44 (q, 4H, NCH_2CH_3, J

=9.2 Hz), 4.75 (s, 2H, OCH_2C=O), 5.97 (s, 2H, Py*H*), 7.06–7.09 (d, 2H, Ar*H*, *J*=8.8 Hz), 7.17–7.19 (d, 2H, Ar*H*, *J*=8.8 Hz), ^{13}C–NMR spectrum (400 MHz, $CDCl_3$, ppm): δ 12.6 (2C, CH_2CH_3), 14.6 (2C, Py*C*H_3), 40.4, 41.8 (2C, NCH_2CH_3), 67.3 (C, OCH_2CO), 115.7, 121.3, 127.4, 129.5 (6C, Ar*C*) 131.6, 141.2, 142.6, 155.0, 158.4, 166.7 (8C, Py*C*) MALDI-TOF MS (m/z): 452.789 (100) calcd : 453.240.

2,2'-[(4-formyl-1,2-phenylene)bis(oxy)]bis(N,N-diethylacetamide), **5b**

A suspension of 3,4-dihydroxybenzaldehyde, **4b** (748 mg, 5 mmol), K_2CO_3 (3.255 g) and 2-chloro-*N*,*N*-diethylacetamide, **3** (2.8 ml, 20 mmol) in CH_3CN 50 ml was refluxed overnight. The solid was removed by filtration. Subsequently, the filtrate was concentrated under reduced pressure resulting in a residue. The residue was dissolved in 100 ml CH_2Cl_2, washed with 0.5 M HCl (100 ml), followed by water (200 ml). After drying with Na_2SO_4, the solvent was removed under reduced pressure. The crude product was purified by column chromatography (silica, 0–5 % MeOH/CH_2C1_2,) the desired product **5** (1.39 g) was obtained as a yellow oil at 77 % yield. ^{1}H-NMR spectrum (400 MHz, $CDCl_3$, ppm): δ 1.11–1.27 (m, 12H, CH_2CH_3, *J*=62.8 Hz), 3.34–3.47 (m, 8H, NCH_2CH_3, *J*=46.8 Hz), 4.82 (s, 2H, OCH_2C=O), 4.88 (s, 2H, OCH_2C=O), 7.04–7.06 (d, 1H, Ar*H*, *J*=8.4 Hz), 7.40 (s, 1H, Ar*H*), 7.45–7.48 (d, 2H, Ar*H*, *J*=10.4 Hz), 9.82 (s, 1H, ArC*H*O).

10-{3,4-bis[2-(diethylamino)-2-oxoethoxy]phenyl}-5,5-difluoro-1,3,7,9-tetramethyl-5H-dipyrrolo[1,2-c:2',1'-f][1–3]diazaborinin-4-ium-5-uide, **BDP2**

2,2′-[(4-Formyl-1,2-phenylene)bis(oxy)]bis(*N*,*N*-diethylacetamide), **5b** (310 mg, 0.75 mmol) and 2,4-dimethylpyrrole (3 ml, 2 mmol) were dissolved in anhydrous CH_2Cl_2 (160 ml) under N_2 atmosphere. Then, one drop of TFA was added to the solution, which was then stirred for 5 h at room temperature. A solution of DDQ, 360 mg, 2.16 mmol) in CH_2Cl_2 was added with a syringe, and the reaction was continued for another 4 h. Then Et_3N (2 ml) was added, followed by BF_3OEt_2 (4 ml) over 30 min then stirring overnight. After concentrating under vacuum, the residue was purified by column chromatography (silica, 10% EtOAc/CH_2C1_2) and the desired product **BDP2** (123 mg) was obtained as a brown solid at 23 % yield. ^{1}H-NMR spectrum (400 MHz, $CDCl_3$, ppm): δ 1.07–1.26 (m, 12H, CH_2CH_3, *J*=73.6 Hz), 1.45 (s, 6H, PyCH_3), 2.55 (s, 6H, PyCH_3), 3.32–3.47 (m, 8H, NCH_2CH_3, *J*=62.4 Hz), 4.74 (s, 2H, OCH_2C=O), 4.83 (s, 2H, OCH_2C=O), 5.97 (s, 2H, Py*H*), 6.78 (s, 1H, Ar*H*), 6.82–6.84 (d, 1H, Ar*H*, *J*=8.4 Hz), 7.08–7.10 (d, 1H, Ar*H*, *J*=8.0 Hz), ^{13}C-NMR spectrum (400 MHz, $CDCl_3$, ppm): δ 12.6, 13.9 (4C, CH_2CH_3), 14.3, 29.4 (4C, PyCH_3), 40.3, 41.5, 41.8 (4C, NCH_2CH_3), 67.9, 68.6 (C, OCH_2CO), 114.0, 115.4, 121.2, 121.6, 128.8 (6C, Ar*C*) 131.6, 141.2, 142.9, 148.4, 149.1, 154.9 166.3, 166.6 (8C, Py*C*) MALDI-TOF MS (m/z): 582.337 (100) calcd : 582.319.

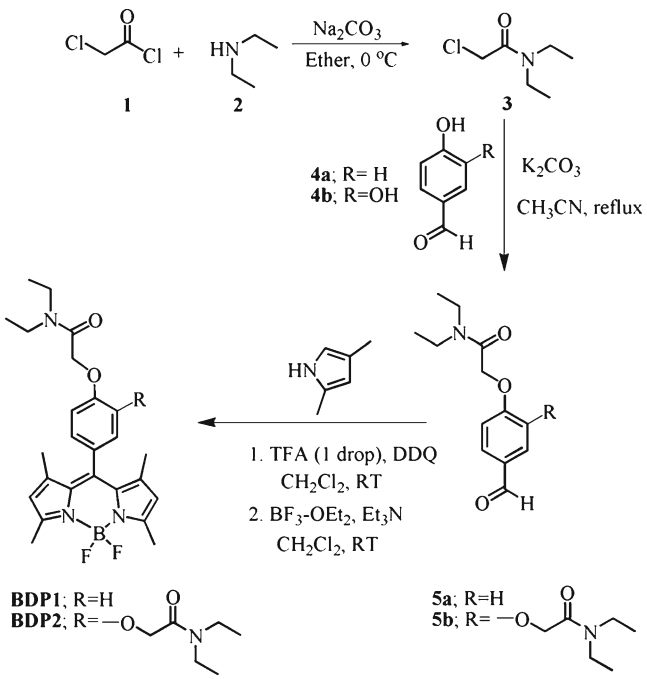

Scheme 1 Synthesis of 4,4-difluoro-4-bora-3a,4a-diaza-s-indacene (BODIPY)-based chemosensors, **BDP1** and **BDP2**

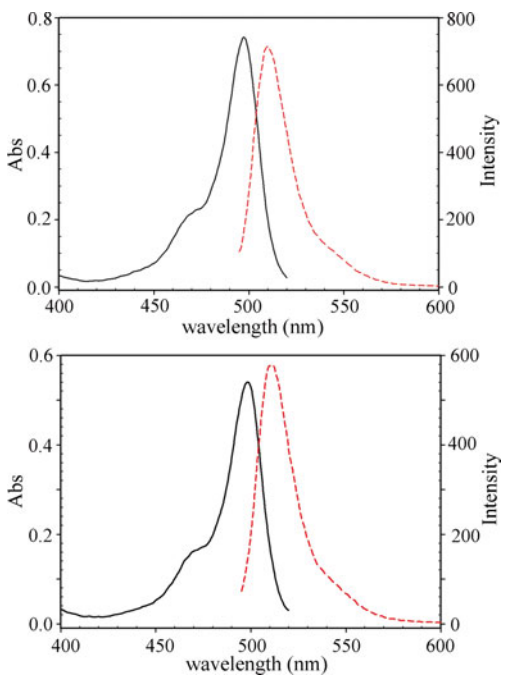

Fig. 1 Absorption (*solid line*) and fluorescence (*dotted line*) spectra of **BDP1** (*top*) and **BDP2** (*bottom*) in dry methanol

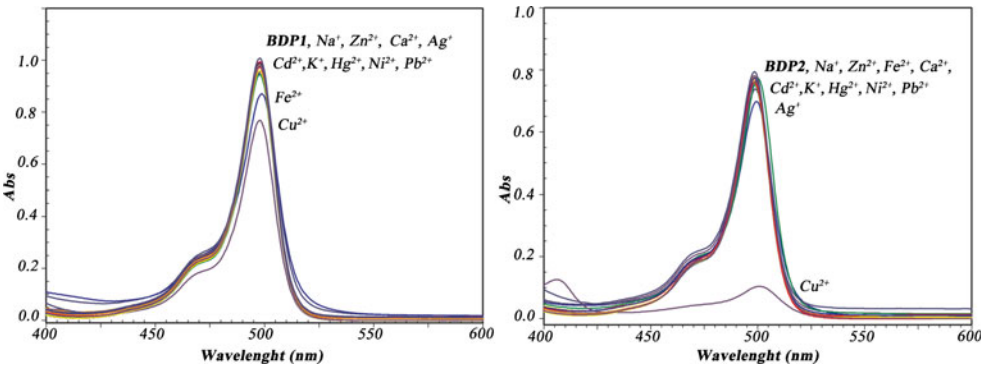

Fig. 2 UV-vis spectrum changes of 1.0×10^{-5} M **BDP1** (*left*) and 1.0×10^{-5} M **BDP2** (*right*) upon addition of various cations (50 equivalent) in dry methanol

Apparatus

Nuclear magnetic resonance (NMR) spectra were recorded on a Varian 400 MHz NMR spectrometer. In all cases, ligands were dissolved in deuterated chloroform ($CDCl_3$). Matrix assisted laser desorption ionization time of flight (MALDI-TOF) mass spectrometer readings were determined on a Bruker Daltonics MALDI-TOF using acetonitrile as solvent (Bruker, http://www.bruker.com). UV-vis titration spectra were measured by a Perkin Elmer Lambda 25 spectrophotometer at 25 °C (Perkin Elmer, http://www.perkinelmer.com). Fluorescence spectra were recorded by Perkin Elmer SL50B fluorescence spectrophotometer with excitation and emission slit set at 5.0 nm.

Computational details

Structures of BODIPY-based chemosensors and their complexes with cation guests, i.e., Na^+, K^+, Ag^+, Hg^{2+}, Ca^{2+}, Pb^{2+}, Fe^{2+}, Ni^{2+}, Cu^{2+}, Zn^{2+} and Cd^{2+} were optimized by DFT. Calculations with the hybrid density functional B3LYP recommended Becke's three-parameter exchange functional [35] with the Lee-Yang-Parr correlation functional, [36] using the Los Alamos LanL2DZ split-valence basis set [37–39]. All calculations were performed using the GAUSSIAN 03 program [40]. Ab initio quantum chemical calculations at correlated second-order Møller-Plesset perturbation theory (MP2/LanL2DZ) level were performed for electronic property calculations of BODIPY derivatives and analysis of their metal ion complexes. The highest occupied molecular orbital (HOMO) and the lowest unoccupied molecular orbital (LUMO) energy gaps were also investigated at the same level of theory. Thermodynamic property changes (ΔX), i.e., total energy (ΔE), enthalpy (ΔH) and Gibbs free energy (ΔG) changes, of complexation in the fully optimized geometry were obtained from Eq. (1).

$$\Delta X = X(\text{chemosensor/cation}) - [X(\text{chemosensor}) + X(\text{cation})] \quad (1)$$

Where X(chemosensor/cation), X(chemosensor) and X(cation) are the thermodynamic properties of the chemosensor/cation complex, free chemosensor and cation, respectively.

In addition, natural bond orbital (NBO) analysis implemented in the GAUSSIAN 03 program was applied through a series of intermolecular interactions under the MP2/LanL2DZ system to evaluate NBO charges.

Results and discussion

Synthesis

This work aimed to synthesize metal ion chemosensors containing organic dyes giving an optical signal. 4-(2-(Diethylamino)-2-oxoethoxy)phenyl (**BDP1**) and 3,4-bis(2-(diethylamino)-2-oxoethoxy)pheny, (**BDP2**)

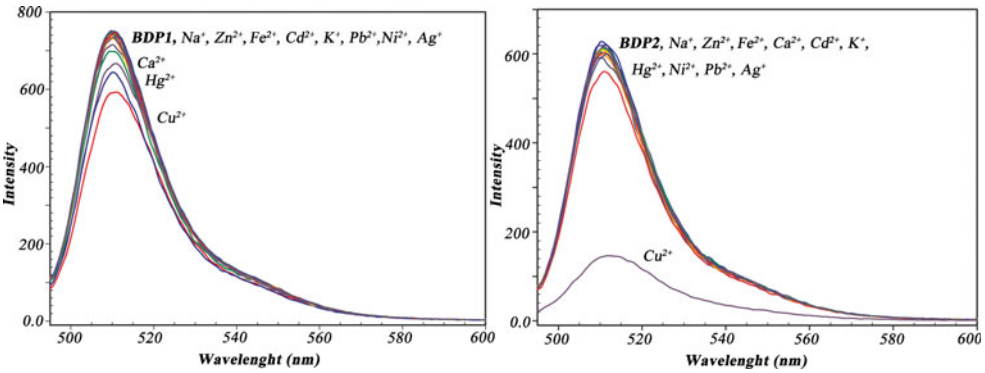

Fig. 3 Fluorescence spectrum changes of 1.0×10^{-7} M **BDP1** (*left*) and 1.0×10^{-7} M **BDP2** (*right*) upon addition of various cations (50 equivalents) in dry methanol (λ_{ex}=485 nm)

Table 1 The zero point vibrational correction energy (ΔE_{ZPE}) and enthalpy (ΔH) and Gibbs free energy (ΔG) changes of complexations between receptors BDP1, BDP2 and metal ions

Metal ions	ΔE_{ZPE} [a]		ΔH [a]		ΔG [a]	
	BDP1	BDP2	BDP1	BDP2	BDP1	BDP2
Na^+	−35.74	−85.73	−14.51	−57.70	−71.31	−129.47
K^+	−20.74	−61.00	0.66	−32.76	−56.39	−105.00
Ag^+	−47.42	−99.83	−26.06	−71.57	−82.26	−142.98
Ca^{2+}	−118.19	−220.40	−96.99	−192.75	−153.42	−262.64
Fe^{2+}	−252.89	−372.90	−233.20	−345.48	−284.11	−414.25
Ni^{2+}	−337.93	−416.18	−316.71	−388.27	−373.10	−459.45
Cu^{2+}	−342.37	−407.02	−321.00	−378.69	−377.40	−451.29
Zn^{2+}	−209.90	−341.46	−190.16	−313.73	−241.16	−383.93
Cd^{2+}	−172.94	−291.50	−152.47	−263.65	−206.36	−333.31
Hg^{2+}	−225.65	−286.75	−204.09	−258.69	−260.90	−328.79
Pb^{2+}	−177.54	−255.36	−156.21	−227.21	−212.23	−297.97

[a] In kcal mol^{-1}

synthesized by coupling appropriate *N*,*N*-diethyl-2-(4-formylphenoxy)acetamide moieties were used as the metal ion binding subunit because they interact effectively with cationic species by electrostatic interaction and contain one or two binding subunits for different metal ions. BODIPY-based signaling units were designed to link directly to the binding subunits; the synthetic pathway is shown in Scheme 1.

Chemosensors **BDP1** and **BDP2** were synthesized in a one-pot reaction modified according to the procedure reported by Gabe et al. [41]. The condensation reaction of benzaldehyde derivatives and 2,4-dimethylpyrrole in the presence of TFA as catalyst was carried out in anhydrous CH_2Cl_2 under N_2 atmosphere. After oxidization with DDQ followed by reacted with BF_3OEt_2, the residue was purified by column chromatography. The desired product **BDP1** was obtained as a red-brown solid at 33 % yield; **BDP2** was obtained at 23 % yield.

Spectroscopic and selective properties

The absorption and fluorescence spectra of **BDP1** and **BDP2** solutions in MeOH (Fig. 1) show the characteristic spectroscopic properties of the BODIPY chromophore with slight Stoke shifts. Both **BDP1** and **BDP2** show a strong S_0–S_1 transition with maximum at 498 nm (ε=94,800 M^{-1} cm^{-1} and ε=78,100 M^{-1} cm^{-1} for **BDP1** and **BDP2**, respectively) [42]. After excitation at 485 nm, the fluorescence spectra of both **BDP1** and **BDP2** display an emission at 510 nm. The fluorescence intensity of **BDP2** is slightly lower than the analogous **BDP1** upon excitation at 485 nm due to the stronger PET process from more oxygen donor atoms in the binding subunits to the BODIPY fluorophore [43]. The optical change of both BODIPY-based chemosensors (1.0×10^{-5} M) was studied by adding of 50 equivalents of various metal ions such as Na^+, K^+, Ag^+, Ca^{2+}, Fe^{2+}, Ni^{2+}, Cu^{2+}, Zn^{2+}, Cd^{2+}, Hg^{2+} and Pb^{2+} ions to the solution of chemosensor in dry

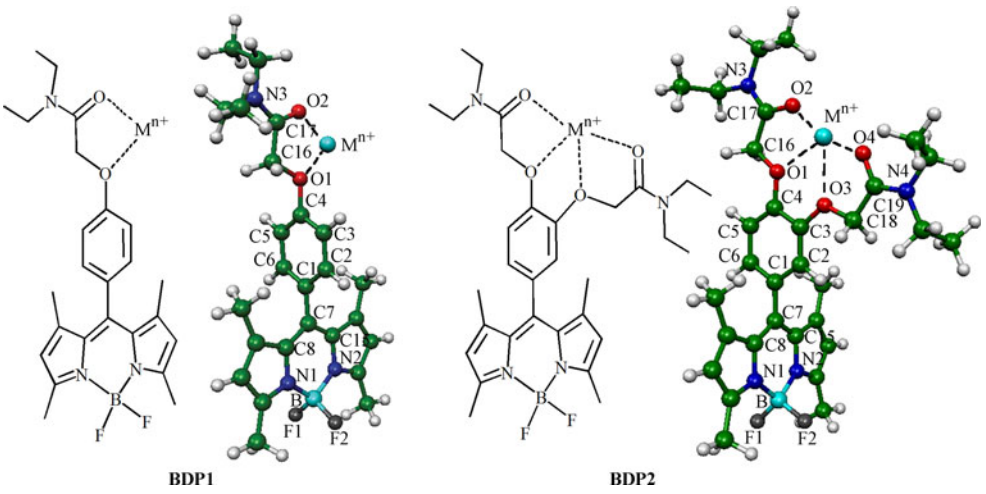

Fig. 4 Chemical -optimized models and atomic labeling of receptor **BDP1** and **BDP2** complexed with metal ions

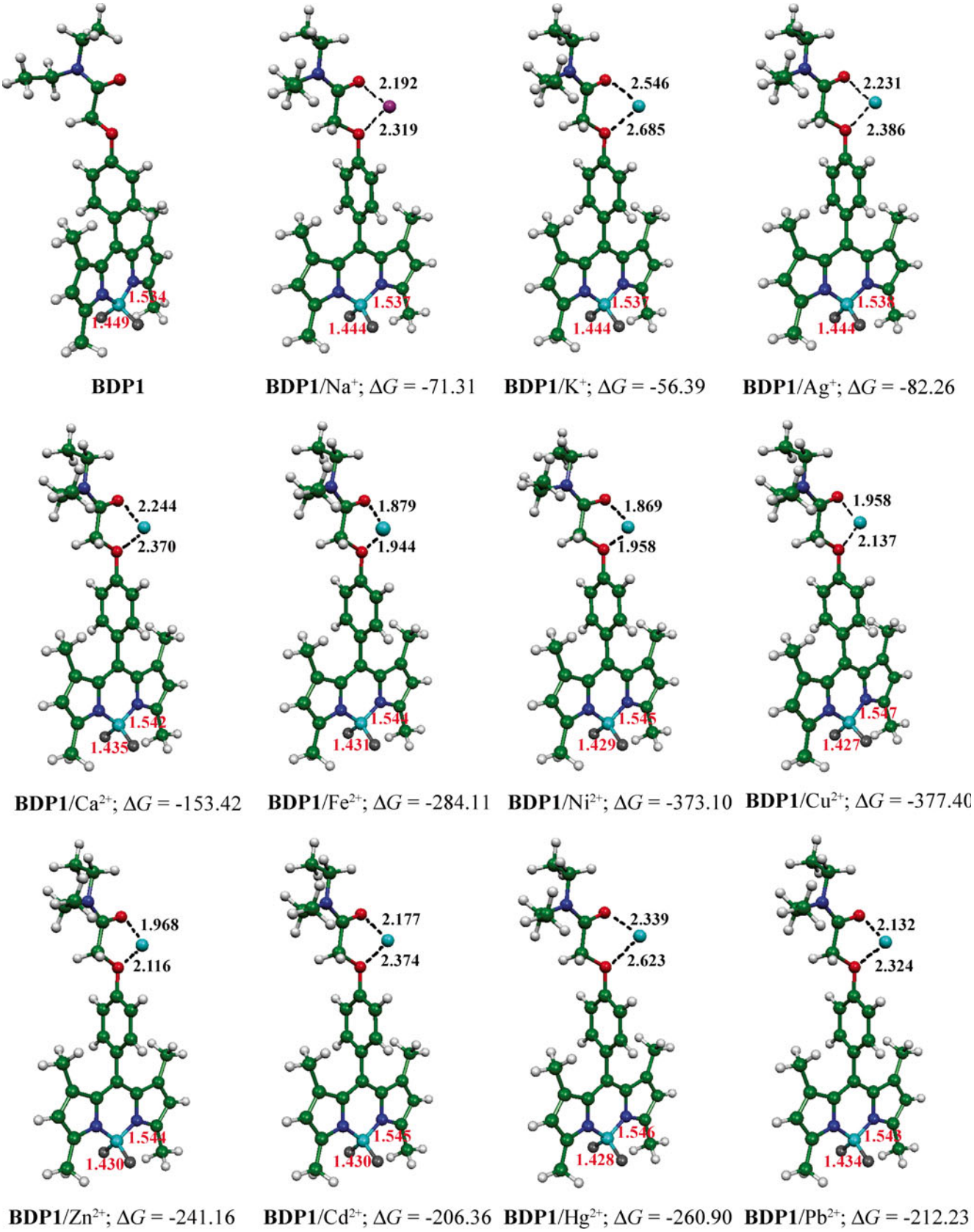

Fig. 5 B3LYP/LanL2DZ-optimized structures of chemosensor **BDP1** and its metal ions complexes. Bond distances and binding free energies are in Ångstroms and kcal mol^{-1}, respectively

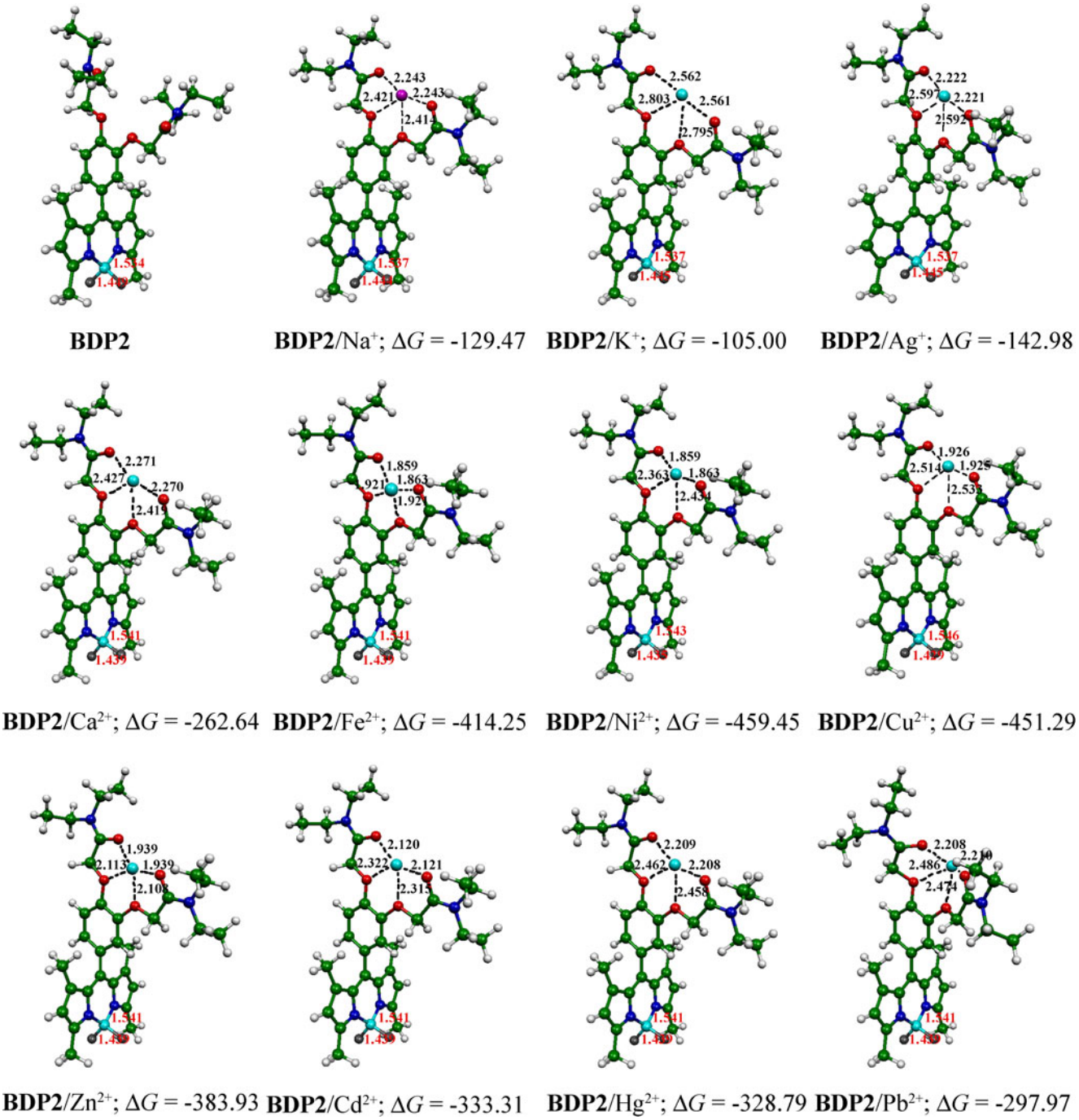

Fig. 6 B3LYP/LanL2DZ-optimized structures of chemosensor **BDP2** and its metal ions complexes. Bond distances and binding free energies are in Ångstroms and kcal mol^{-1}, respectively

methanol. The spectral changes of **BDP1** and **BDP2** are shown in Fig. 2. Free **BDP1** and **BDP2** both show an absorption band center at 498 nm. After addition of the metal ion, the absorption at 498 nm is decreased (most pronounced for **BDP2**/Cu^{2+} ion; ε=10,100 M^{-1} cm^{-1}).

The fluorescence behavior of synthetic chemosensors and their complexes with an excess of metal ions was also investigated (λ_{ex} at 485 nm, λ_{em} 490–600 nm). The fluorescence spectra of **BDP1** and **BDP2** (1.0×10^{-7} M in MeOH) in the absence and presence of 50 equivalents of various metal ions are shown in Fig. 3. Both spectra revealed Cu^{2+} ion to be the most efficient in quenching, especially in **BDP2**. The quantum yields were estimated to be 4-fold (Φ_0/Φ=4.222) quenching for **BDP2** and 2-fold (Φ_0/Φ=1.211) quenching for **BDP1**. In contrast, the fluorescence intensity of **BDP2** is almost not influenced by the addition of other metal ions.

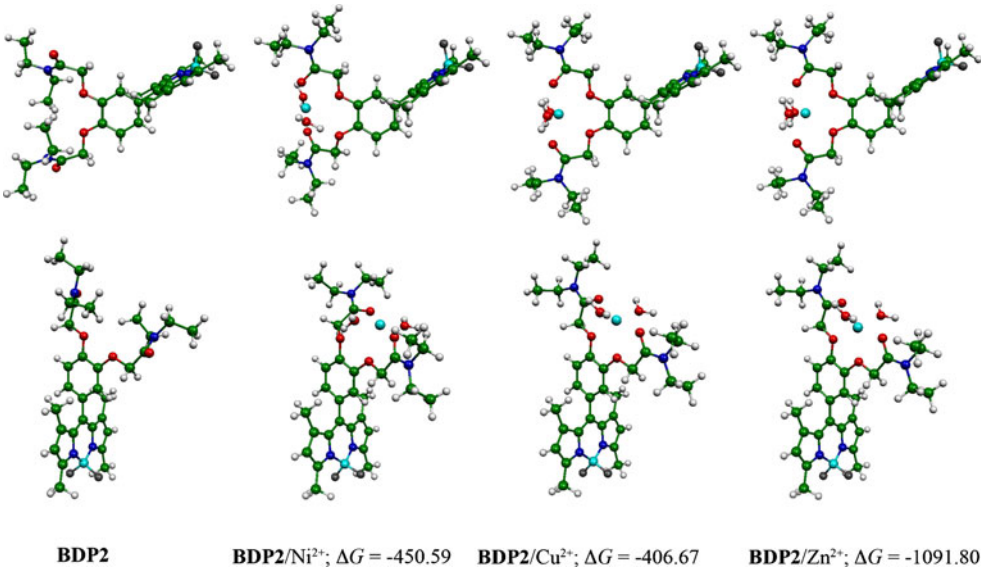

Fig. 7 B3LYP/LanL2DZ-optimized structures of the chemosensor **BDP2** and its metal ion complexes with saturated metal coordination by H_2O solvent molecules. Bond distances and binding free energies are in Ångstroms and kcal mol^{-1}, respectively

Binding energies of chemosensors **BDP1**, **BDP2** and their complexations with various cations

The most important parameter used to predict metal ion selectivity is changes in either Gibbs free energy (ΔG) or binding energies of complexation. The Gibbs free energy changes of **BDP1** and **BDP2** for metal ion complexes in vaccuo were computed. The computed values of binding energies, binding enthalpies and Gibbs free energies are listed in Table 1. The binding energies of both **BDP1** and **BDP2** with metal ions indicated that binding occurred via exothermic processes. The **BDP1** and metal ion binding strengths are, in decreasing order: **BDP1**/Cu^{2+} ~ **BDP1**/Ni^{2+} > **BDP1**/Fe^{2+} > **BDP1**/Hg^{2+} > **BDP1**/Zn^{2+} > **BDP1**/Cd^{2+} ~ **BDP1**/Pb^{2+} > **BDP1**/Ca^{2+} > > **BDP1**/Ag^{+} > **BDP1**/Na^{+} > **BDP1**/K^{+}.

For **BDP2**, the trend of the binding energy with different metal ions also shows the highest selectivity to Cu^{2+} ion. The binding strengths for **BDP2** and metal ions are in decreasing order: **BDP2**/Cu^{2+} ~ **BDP2**/Ni^{2+} > **BDP2**/Fe^{2+} > **BDP2**/Zn^{2+} > **BDP2**/Cd^{2+} ~ **BDP2**/Hg^{2+} > **BDP2**/Pb^{2+} > **BDP2**/Ca^{2+} > **BDP2**/Na^{+} ~ **BDP2**/Ag^{+} > **BDP2**/K^{+}.

Geometries of chemosensors **BDP1**, **BDP2** and their complexations with various cations

The chemical, optimized models and atomic labeling of chemosensors **BDP1** and **BDP2** complexes with metal ions are shown in Fig. 4. The B3LYP/LanL2DZ optimized structures of **BDP1** and **BDP2** and their complexes with metal ions are shown in Figs. 5 and 6, respectively. The selected

Table 2 Selected natural bond orbital (NBO) charge (in *e*) analysis of metals in complexes **BDP1** and **BDP2** computed at the MP2/LanL2DZ level

Atom no.	BDP1	BDP1/Cu^{2+}	BDP1/Zn^{2+}	BDP2	BDP2/Cu^{2+}	BDP2/Zn^{2+}	BDP2/Ni^{2+}
N1[a]	−0.718	−0.733	−0.707	−0.718	−0.736	−0.712	−0.712
N2[a]	−0.718	−0.733	−0.713	−0.718	−0.736	−0.712	−0.711
B[a]	1.458	1.449	1.457	1.458	1.449	1.457	1.456
F1[a]	−0.637	−0.614	−0.626	−0.635	−0.619	−0.632	−0.632
F2[a]	−0.636	−0.614	−0.626	−0.636	−0.614	−0.623	−0.622
N3[a]	−0.631	−0.577	−0.557	−0.611	−0.592	−0.562	−0.549
O1[a]	−0.728	−0.683	−0.774	−0.648	−0.643	−0.734	−0.705
O2[a]	−0.626	−0.908	−0.958	−0.612	−0.593	−0.561	−0.549
N4[a]				−0.649	−0.642	−0.735	−0.696
O3[a]				−0.765	−0.838	−0.945	−0.933
O4[a]				−0.764	−0.843	−0.942	−0.953
OW1[b]		−1.160	−1.087		−1.027	−1.085	−1.083
OW2[b]		−1.049	−1.085		−1.027	−1.085	−1.048
OW3[b]		−1.046	−1.092				
OW4[b]		−1.067	−1.077				
M[c]		0.921	1.854		0.922	1.851	1.614

[a]N1, N2, B, F1, F2, O1, O2, N3, N4, O3 and O4 are atoms on the receptor **BDP1** and **BDP2** which are defined in Fig. 4

[b]OW1, OW2, OW3 and OW4 are atoms on the explicit H_2O solvent molecules

[c]M is metal ion on the complexes **BDP1** and **BDP2** which are defined in Fig. 6

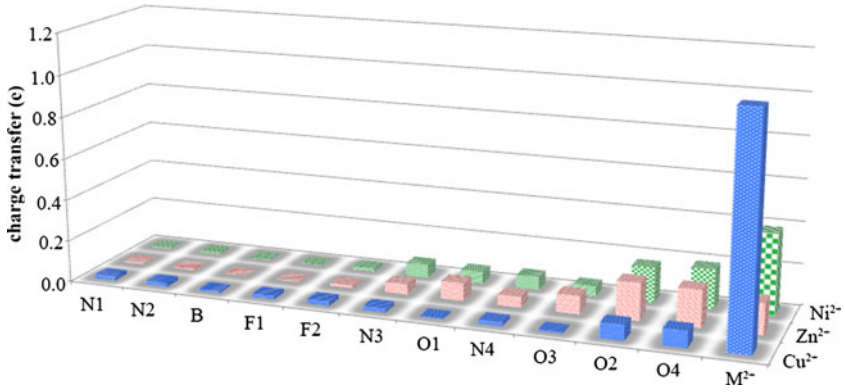

Fig. 8 Natural bond orbital (NBO) charge transfer of **BDP2**/Cu^{2+}·$2H_2O$, **BDP2**/Zn^{2+}·$2H_2O$ and **BDP2**/Ni^{2+}·$2H_2O$ complexed calculated at MP2/LanL2DZ level of theory

geometrical parameters of the data of all optimized structures are listed in Tables S1 and S2. The complexations of **BDP1** and **BDP2** with metal ions show the significant change in their structures. Specifically, the metal ion complexation induces a more symmetrical structure than that of the free chemosensor; for **BDP2** binding subunits especially, alignment of the metal ion depends on the common metal ion geometry.

To determine whether the solvent molecule alters the geometry significantly or not, some metal complexes were chosen for optimization as saturated coordination spheres. The structure of **BDP2**/Cu^{2+}, **BDP2**/Ni^{2+} and **BDP2**/Zn^{2+} complexes with two water molecules optimized at the B3LYP/LanL2DZ level of theory are shown in Fig. 7. The presence of two water molecules with four oxygen donor atoms of the binding subunit of **BDP2** results in a distorted tetragonal geometry. The average N1-B and N2-B bond lengths of metal ion complexes of both chemosensors are longer than the N1-B and N2-B bond lengths (1.534 Å) of the free chemosensor. The Cu^{2+} complex, especially, has the longest average N1-B and N2-B bond lengths (1.542 Å). The average F1-B and F2-B bond lengths of metal ion complexes of both chemosensors are shorter than the F1-B and F2-B bond lengths (1.449 Å) of the free chemosensor. The Cu^{2+} complex has the shortest average F1-B and F2-B bond lengths (1.436 Å). The N1-B-N2 bond angles of the complexes are smaller than the N1-B-N2 bond angles (108.3 Å) of the free chemosensors but the F1-B-F2 bond angles of the complexes are bigger than the F1-B-F2 bond angles (107.3 Å) of the free chemosensors. From these data, it is evident that metal ion complexation at the binding subunit affects not only the bond length within the binding

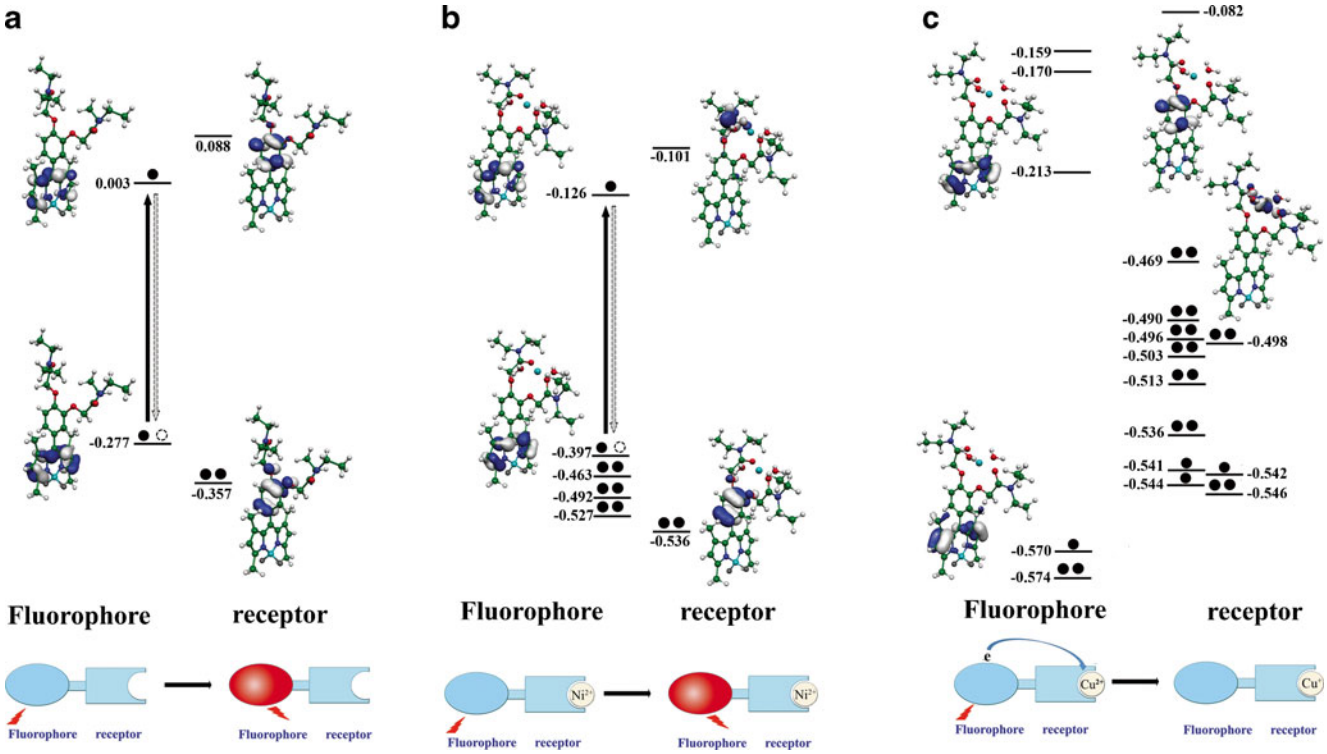

Fig. 9 Frontier orbital energy level diagrams and electron-transfer paths in **BDP2** (**a**), **BDP2**/Ni^{2+} (**b**) and **BDP2**/Cu^{2+} (**c**) complexes

subunit itself but also the bond length within the signaling subunit.

Electronic properties and partial charge transfer

The electron density of **BDP1** and **BDP2** and **BDP2**/Cu^{2+}, **BDP2**/Ni^{2+} and **BDP2**/Zn^{2+} complexes in saturated coordination sphere complexes were calculated using MP2/LanL2DZ level of theory. The NBO charges on selected atoms of free **BDP1** and **BDP2** and their metal ion complexes are listed in Table 2. From these data, the NBO charges of selected atoms of oxoethoxy phenyl amide binding subunits and the BODIPY chromophore subunit are significantly changed. These results indicate that metal ion recognition via ion–dipole interactions induces a charge transfer process from not only oxoethoxy phenyl amide binding subunits to the metal ion but also from the BODIPY chromophore subunit. The absolute NBO charge changes are presented in Fig. 8. In the case of the ligand to metal charge transfer (LMCT), the complexation of Cu^{2+} ion and **BDP2** shows the highest LMCT. This result indicates that Cu^{2+} is capable of single-electron reduction from Cu^{2+} to Cu^{+} ion.

The energy level of the corresponding molecular orbitals (MO), as first developed by Weller [44], can provide a clue to the quenching process in fluorescence emission experiments. Following Weller's approach, the HOMO–LUMO electron distributions were computed on the total system. The donor orbitals and acceptor orbitals were distinguished by simply inspecting the orbital distribution diagram. The frontier orbital energy level diagrams and electron-transfer paths in **BDP2**, **BDP2**/Ni^{2+} and **BDP2**/Cu^{2+} complexes were chosen to illustrate this process, as shown in Fig. 9. First, we considered electron transfer processes in the free chemosensor **BDP2** (Fig. 9a). After excitation, the excited electron is able to go back to the ground state. Therefore, free chemosensor is able to exhibit fluorescence. The same is true for the **BDP2**/Ni^{2+} complex (Fig. 9b).

For Cu^{2+} ion, complexation leads to the transfer of electrons from **BDP2** to the Cu^{2+} ion in a mechanism known as one-electron reduction process, as depicted in Fig. 9c. The picture also shows that, after the electron transfer process, Cu^{2+} is reduced to Cu^{+} ion, while the ground state MO of the signaling subunit is a singly occupied molecular orbital (SOMO) and all 3d orbitals of copper are doubly occupied (HOMO1–HOMO5). Accompanying this is the wider energy gap of **BDP2**. The complex is now unable to be excited by a photon of the energy able to excite the free chemosensor. That is, the Cu^{2+} ion decreases in absorbance as well as quenching the fluorescence emission intensity.

Conclusions

Two BODIPY derivatives containing 4-[2-(diethylamino)-2-oxoethoxy]phenyl (**BDP1**) and 3,4-bis[2-(diethylamino)-2-oxoethoxy]phenyl (**BDP2**) were designed and synthesized for use as metal ion chemosensors. The one-pot reaction of benzaldehyde derivative and 2,4-dimethylpyrrole in the presence of TFA as catalyst was modified for synthesis of these chemosensors. The binding abilities between synthetic chemosensors and 50 equivalents of Na^{+}, K^{+}, Ag^{+}, Ca^{2+}, Fe^{2+}, Ni^{2+}, Cu^{2+}, Zn^{2+}, Cd^{2+}, Hg^{2+} and Pb^{2+} ions in methanol were studied using UV-vis and fluorescence spectrophotometric methods. The results show the decrease in both UV-vis absorption and fluorescence emission intensity when both **BDP1** and **BDP2** complexed with Cu^{2+} ion. The structure of free **BDP1**, **BDP2** and their complexes with Na^{+}, K^{+}, Ag^{+}, Ca^{2+}, Fe^{2+}, Ni^{2+}, Cu^{2+}, Zn^{2+}, Cd^{2+}, Hg^{2+} and Pb^{2+} ions in vaccuo were optimized using DFT calculations at B3LYP/LanL2DZ. The saturated coordination spheres with two water solvent molecules of **BDP2**/Cu^{2+}, **BDP2**/Ni^{2+} and **BDP2**/Zn^{2+} complexes were also optimized at the same level of theory. The electronic properties of the BODIPY derivatives and their metal ion complexes were calculated at second-order Møller-Plesset perturbation theory level (MP2/LanL2DZ). The calculations show that copper ions can quenched fluorescence due to the single-electron reduction process with reduction of Cu^{2+} to Cu^{+} ion.

Acknowledgments The authors gratefully acknowledge the Faculty of Science, Mahasarakham University and the Center of Excellence for Innovation in Chemistry (PERCH-CIC), Thailand for financial support of this research, and the facilities provided by the Supramolecular Chemistry Research Unit and Department of Chemistry, Faculty of Science, Mahasarakham University.

References

1. de Silver AP, Gunaratne HQN, Gunnlaugsson T, Huxley AJM, McCoy CP, Rademacher JT, Rice TE (1997) Chem Rev 97:1515–1566
2. Fabbrizzi L, Poggi A (1995) Chem Soc Rev 24:197–202
3. Koumoto K, Takeuchi M, Shinkai S (1998) Supramol Chem 9:203–210
4. Gooding JJ, Hibbert DB, Yang W (2001) Sensors 1:75–90
5. Çeken B, Kandaz M, Koca A (2012) Synth Met 162:1524–1530
6. Shaabani B, Shaghaghi Z, Khandar AA (2012) Spectros Chim Acta A Mol Biomol Spectros 98:81–85
7. Berdnikova DV, Fedorov YV, Fedorova OA (2013) Dyes Pigm 96:287–295
8. Cozar O, Leopold N, Jelic C, Chis V, David L, Mocanu A, Tomoaia-Cotisel M (2006) J Mol Struct 788:1–6
9. Leopold N, Szabó L, Pîrnau A, Aluasß M, Leopold LF, Chißs V, Cozar O (2009) J Mol Struct 919:94–99
10. Szabó L, Herman K, Mircescu NE, Falamas A, Leopoldc LF, Leopold N, Buzumurga C, Chis V (2012) Spectros Chim Acta A Mol Biomol Spectros 93:266–273
11. Szabó L, Herman K, Leopold N, Buzumurga C, Chis V (2011) Spectros Chim Acta A Mol Biomol Spectros 79:226–231
12. Demchenko AP (2009) Introduction to fluorescence sensing. Springer, Dordrecht
13. Valeura B, Leraya I (2000) Coord Chem Rev 205(1):3–40
14. Jeong Y, Yoon J (2012) Inorg Chim Acta 381:2–14

15. Kaur N, Kumar S (2011) Tetrahedron 67:9233–9264
16. Dong M, Ma TH, Zhang AJ, Dong YM, Wang YW, Peng Y (2010) Dyes Pigm 87:164–172
17. Bhalla V, Kumar R, Kumar M, Dhir A (2007) Tetrahedron 63:11153–11159
18. Kumar R, Bhalla V, Kumar M (2008) Tetrahedron 64:8095–8101
19. Li Y, Du J, Zhang P, Ding J (2010) J Struct Biol 169:399–405
20. Finney LA, O'Halloran TV (2003) Science 300(5621):931–936
21. Šukalović VHT, Vuletić M, Veljović-Jovanović S, Vučinić Ž (2010) J Plant Physiol 167:1550–1557
22. Arnal N, de Alaniz MJT, Marra CA (2012) Biochim Biophys Acta 1820:931–939
23. Kang YJ (2011) Pharm Ther 129:321–331
24. Linder MC (2012) Mutat Res 733:83–91
25. Vinkenborga JL, Koaya MS, Merkx M (2010) Curr Opin Chem Biol 14:231–237
26. Liu WY, Li HY, Lv HS, Zhao BX, Miao JY (2012) Spectros Chim Acta A Mol Biomol Spectros 95:658–663
27. Benstead M, Mehl GH, Boyle RW (2011) Tetrahedron 67(20):3573–3601
28. Suzuki S, Kozaki M, Nozaki K, Okada K (2011) J Photochem Photobiol C Photochem Rev 12(4):269–292
29. Boens N, Leen V, Dehaen W (2012) Chem Soc Rev 41:1130–1172
30. Ulrich G, Ziessel R, Harriman A (2008) Angew Chem Int Ed 47:1184–1201
31. Lu H, Zhang SS, Liu HZ, Wang YW, Shen Z, Liu CG, You XZ (2009) J Phys Chem A 113(51):14081–14086
32. Bozdemir OA, Guliyev R, Buyukcakir O, Selcuk S, Kolemen S, Gulseren G, Nalbantoglu T, Boyaci H, Akkaya EU (2010) J Am Chem Soc 132(23):8029–8036
33. Atilgan S, Ozdemir T, Akkaya EU (2010) Org Lett 12(21):4792–4795
34. Li Q, Guo Y, Shao S (2012) Sens Actuators B: Chem (171–172): 872–877
35. Becke AD (1993) J Chem Phys 98:5648–5652
36. Lee C, Yang W, Parr RG (1988) Phys Rev B 37:785–789
37. Hay PJ, Wadt WR (1985) J Chem Phys 82:270–283
38. Wadt WR, Hay PJ (1985) J Chem Phys 82:284–298
39. Hay PJ, Wadt WR (1985) J Chem Phys 82:299–310
40. Frisch MJ, Trucks GW, Schlegel HB, Scuseria GE, Robb MA, Cheeseman JR, Montgomery JA, Vreven T, Kudin KN, Burant JC, Millam JM, Iyengar SS, Tomasi J, Barone V, Mennucci B, Cossi M, Scalmani G, Rega N, Petersson GA, Nakatsuji H, Hada M, Ehara M, Toyota K, Fukuda R, Hasegawa J, Ishida M, Nakajima T, Honda Y, Kit Ao O, Nakai H, Klene M, Knox JE, Hratchian HP, Cross JB, Adamo C, Jaramillo J, Gomperts R, Stratmann RE, Yazyev O, Austin AJ, Cammi R, Pomelli C, Ochterski JW, Ayala PY, Morokuma K, Voth GA, Salvador P, Dannenberg JJ, Zakrzewski VG, Dapprich S, Daniels AD, Strain MC, Farkas O, Malick DK, Rabuck AD, Raghavachari K, Foresman JB, Ortiz JV, Cui Q, Baboul AG, Clifford S, Cioslowski J, Stefanov BB, Liu G, Liashenko A, Piskorz P, Komaromi I, Martin RL, Fox DJ, Keith T, Al-Laham MA, Peng CY, Nanayakkara A, Challacombe M, Gill PMW, Johnson B, Chen W, Wong MW, Gonzalez C, Pople JA (2008) Gaussian 03, Revision E01. Gaussian Inc, Wallingford
41. Baruah M, Qin W, Basarić N, De Borggraeve WM, Boens N (2005) J Org Chem 70(10):4152–4157
42. Kennedy DP, Kormos CM, Burdette SC (2009) J Am Chem Soc 131:8578–8586
43. Gabe Y, Urano Y, Kikuchi K, Kojima H, Nagano T (2004) J Am Chem Soc 126:3357–3367
44. Weller A (1968) Pure Appl Chem 16:115–124